Mechanics of Advanced Composite Structures 11 (2024) 119 – 130
This is an Open Access paper licensed under the Creative Commons License CC-BY 4.0 license.

Semnan University

Mechanics of Advanced Composite Structures

journal homepage: https://MACS.journals.semnan.ac.ir

Elastoplastic Analysis of Pressurized FG Rotating Thick Cylinders Based on High-Order Shear Deformation Theory and Radial Return Method

M. Ghadimi, M. Ghannad *

Department of Mechanical Engineering, Shahrood University of Technology, Shahrood, Iran

KEYWORDS

Elastoplastic analysis;
Shear deformation theory;
Prandtl-Reuss flow rule;
Radial return method;
Thick cylindrical structure.

ABSTRACT

In this paper, the elastoplastic behavior of a rotating thick cylinder is investigated. High-order shear deformation theory (HSDT) is used to define the displacement field. The cylinder is considered to be fixed at both ends and rotates around its axis with specific angular velocity. The cylinder is also made of functionally graded material (FGM), and the properties of the material are changed gradually from the inner to the outer surface. The material is supposed to be elastic-perfectly plastic and the von Mises yield criterion is used to define the state of stress. The Prandtl-Reuss flow rule is used to express the stress-strain relation in the plastic region. The radial return mapping method is applied to compute the elastoplastic stress field. The equilibrium equations and general boundary conditions of the cylinder are derived using the energy method. The elastic limit pressure and the stress analysis of the FG rotating thick cylinders have been obtained by solving the equations derived based on HSDT. The influence of the inhomogeneity constants and angular velocity of the cylinder are studied. The results are evaluated with the finite element method using Abaqus software. The main novelty of the study is investigating shear stress in the elastoplastic analysis of cylindrical shells. The results revealed that using the HSDT with the radial return mapping method has enough accuracy for the elastoplastic analysis of clamped-clamped thick cylindrical structures.

1. Introduction

Functionally graded materials (FGMs) are the advanced category of heterogeneous composite materials with broad applications in industrial engineering. Unlike composite materials, FGMs can tolerate high temperatures without delamination. In addition, the FGMs can be used to reduce stress concentration by controlling the pressure, corrosion, wear, and deformation [1]. Cylindrical structures are one of the most applicable structures in advanced engineering structures especially, in the military, nuclear, and aerospace industries such as missiles, submarines, satellites, aircraft, etc. [2].

Many researchers have studied the thick-walled cylinder behavior subjected to loads. They have not only focused on the elastic behavior of the cylindrical structure. Still, they have extended their studies to elastoplastic behavior to decrease material usage and reduce structure costs by optimizing the design of cylinders. There are many approaches to dealing with the elastic part of thick cylindrical shells and finding the equilibrium equations of the problem. The simplest way is to use the classic theory known as plane elasticity theory (PET) [3-5]. PET can only be appropriate for stress and displacement analysis of the shell through the thickness and therefore is not applicable near the boundaries of the shell. There is another approach, researchers apply to find the equilibrium equations of thick-walled cylindrical shells is shear deformation theory (SDT). For the first time, the analysis of isotropic cylinders was studied by Mirsky and Hermann [6]. They employed first-order shear deformation theory (FSDT), which is also known as the Mirsky-Hermann theory. Later, Reddy and

* Corresponding author. Tel.: +98-23-32300240-3340; fax: +98-23-32300258.
E-mail address: mghannadk@shahroodut.ac.ir & ghannad.mehdi@gmail.com

DOI: 10.22075/macs.2023.30361.1498
Received 2023-04-12; Received in revised form 2023-07-18; Accepted 2023-08-15.
© 2024 Published by Semnan University Press. All rights reserved.

Liu [7] expanded the third-order shear deformation theory to study the shell's behavior. They supposed that the transverse shear strains are parabolically distributed through the shell. For elastic analysis of thick cylinders under external and internal pressures, a formulation based on FSDT was derived by Ghannad and Zamani-Nejad [8] using the virtual work principle. Eipakchi et al. [9] applied FSDT to achieve the governing equations of variable thickness cylinders. They used perturbation theory to solve the equations. They also performed first-order and second-order shear deformation theories for the analysis of a thick conical shell subjected to a non-uniform internal pressure [10].

In addition, there are some works on the elastic analysis of cylinders made of FGMs. Displacement and stress fields of FGM thick cylindrical shells subjected to internal and external pressures were investigated by Ghannad and Gharooni [11] based on the high-order shear deformation theory (HSDT). Elastic analysis of thick FGM conical shells with both ends clamped boundary conditions performed by Ghannad et al. [12]. The conical shells are assumed to be axisymmetric and under internal loading. Ghannad et al. [13] analyzed the stresses and displacements of thick FGM cylinders under internal pressure. They used FSDT and supposed the cylinder to be clamped at both ends. Elastic analysis of truncated conical shells with variable thickness under thermo-mechanical loading was studied by Jabbari et al. [14]. They supposed that the shells were made of FGMs, and they used HSDT for the displacement field of the shell. Gharooni and Ghannad [15] used FSDT to achieve the governing equations of thick hyperelastic cylindrical shells subjected to non-uniform pressure. They used the match asymptotic expansion method for solving the obtained equations of clamped-clamped cylinders. They also solved a similar problem for the cylinders made of FGMs in a radial direction [16]. Parhizkar Yaghoobi and Ghannad used FSDT as well as first-order electric potential theory and applied the energy method to formulate the electro-elasticity of the FGM cylinders. They solved the obtained differential equations system using the classical eigenvalue problem [17].

Furthermore, some researchers studied the elastoplastic behavior of disks, shafts, and shells under simplified hypotheses based on different theories. Nadai [18] analyzed the perfectly plastic rotating cylinders under the assumption of incompressibility. Chakrabarty [19] presented the analytical solution for the elastoplastic expansion of a thick-walled tube subjected to internal pressure based on the Tresca and the von Mises yield criteria. He assumed the tube was so large that transverse plane sections remained plane during the expansion. The elastoplastic deformations of a rotating shaft based on the Tresca yield condition, with linear hardening plasticity and different boundary conditions, were investigated by Eraslan [20]. He also used plane stress theory and the linear strain hardening model of plasticity to study the analytical solution of rotating parabolic disks based on the associated flue rule of the Tresca yield criterion [21]. The elastoplastic analysis of the rotating cylinder subjected to mechanical loading and unloading under plane strain conditions was investigated by Prokudin [22]. Zamani-Nejad et al. [23] developed the elastoplastic analysis of rotating FGM disks by assuming perfectly plastic material behavior. They employed the Tresca yield criterion to predict the plastic state of the material. The elastoplastic solutions for double-layered and multilayered combined thick-walled cylinders under internal pressure were studied by Zhu et al. [24] with unified strength theory, which fully considers the influence of the intermediate principal stress and strength difference. Temesgen et al. [25] analytically and numerically studied the elastoplastic behavior of thick-walled rotating cylindrical shells made of FGMs under thermo-mechanical loading based on Seth transition theory which does not require yield criterion.

Zamani-Nejad et al. [26] presented an analytical solution to analyze the thermo-elastoplastic response of the rotating cylindrical pressure vessel. They assumed the plane strain condition and used the flow rule under the assumption of perfectly plastic material behavior to formulate six different plastic regions using the Tresca yield criterion. In addition, Ebrahimi et al. [27] studied the same problem under the linearly hardening condition.

The class of elastic-predictor plastic-corrector algorithms is based on a two-step scheme: (i) an elastic trial state is first computed; (ii) then, if the onset of plasticity is detected, a plastic correction is computed using the trial state as the initial condition to update all the internal variables [26]. The idea of such a scheme traces back to Wilkins [28], who proposed the radial return method for the von Mises perfect plasticity. The superiority of the radial return mapping method compared to other return schemes is established in the work done by researchers [30, 31]. Dunne and Petrinic [30] applied the radial return method, which is an implicit integration technique, for plasticity problems. They used the normality hypothesis and associated flow rule for the von Mises criterion to formulate the plasticity problems. Widlak [33] presented the radial return method for the elastoplastic constitutive equations in the

particular case analysis of a thick-walled cylinder. The robustness and step-size insensitivity of this integration method were proven, and efficient solution strategies were chosen. Kang et al. [34] improved the radial return mapping algorithm for inelastic structures, including shape memory alloys, to solve the obtained nonlinear differential equations.

In this paper, the elastoplastic stress analysis of the thick-walled rotating cylinders, which are made of functionally graded materials, is investigated. It is supposed that the properties of the cylinder are changed through the thickness of the shell. The displacement field of the cylinder is considered based on high-order shear deformation theory. The cylinder is assumed to be made of elastic-perfectly plastic material. The von Mises yield criterion and Prandtl-Reuss flow rule are applied to find the behavior of the cylinder in the plastic region. The radial return method is applied to solve the elastoplastic stress field of the material. The innovation of this study is the simultaneous use of the HSDT displacement field and radial return method, which is based on the von Mises criterion, for the elastoplastic analysis of cylindrical shells. The case study solved for a clamp-clamp thick cylinder subject to uniform internal pressure that rotates around its longitudinal axis. The elastic limit pressure and the elastoplastic stresses of the cylinder are calculated based on HSDT and other described assumptions of the problem. In addition, to verify the solution, the results are compared with the finite element results obtained by Abaqus.

2. Description of the Problem

Figure 1 shows a cross-section of a cylindrical shell with the inner radius of r_i, the outer radius of r_o, the thickness of h, and the length of L. The position of any typical point m of the cylindrical shell can be defined as follows:

$$m: (r\ , x) = (R + z\ , x)$$
$$-h/2 \le z \le +h/2\ \ ,\ \ 0 \le x \le L \tag{1}$$

where R and z denote the radius of the mid-plane and the distance from the mid-plane, respectively.

As shown in Fig. 1, the cylinder is supposed to be clamped at both ends. In addition, the cylinder tolerates internal pressure P and centrifugal force due to its rotation around its axis. Furthermore, the cylinder made of FGM and the properties of the material, which are changed through the thickness of the cylinder are assumed to be as follows:

$$\mathrm{B}(r) = \mathrm{B}_i \left(\frac{r}{r_i}\right)^n = \mathrm{B}_i \left(\frac{R+z}{r_i}\right)^n \tag{2}$$

where B is the material properties, B_i is the material properties at the inner layer of the cylinder, and n is the inhomogeneity constant. Thus, based on Eq. (2) if the inhomogeneity constant is equal to zero, the cylinder is assumed to be homogenous, and hence the material properties are the same all over the shell.

Contrary to reality, the inhomogeneity constant for all properties of the material is assumed to be the same for the simplicity of the problem. The changes in material properties, such as Young's Modulus, density, and yield limit, are equal to Eq. (2). It is noticeable that Poisson's ratio of the cylinder is assumed to be constant. As demonstrated in Fig. 2, the material properties ratio (B/B_i) enhances or reduces gradually by increasing or decreasing of inhomogeneity constant, respectively.

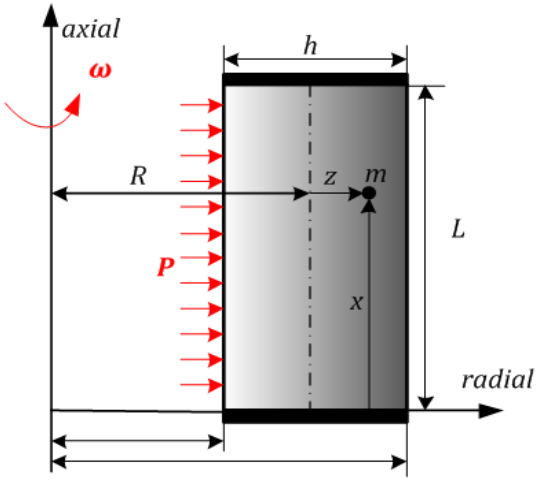

Fig. 1. Cross section of the FGM cylindrical structure

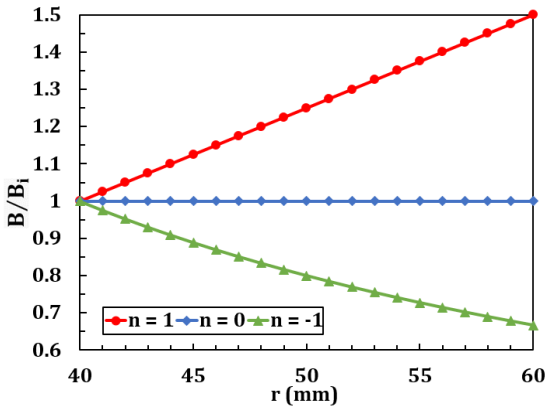

Fig. 2. Material properties ratio changes through the thickness of the cylinder

3. Elastoplastic Analysis of the FG Rotating Cylinder

In this section, the elastoplastic analysis of an FG rotating cylindrical shell is presented. Based on FSDT, the shear stress is uniform throughout the thickness of the cylinder. In reality, the shear

stress is parabolic throughout the thickness of the cylinder. Thus, this theory is not accurate near the boundaries away from the mid-plane of the cylinder. The high-order shear deformation theories can produce parabolic behavior to satisfy tangential traction-free conditions away from the mid-plane of the cylinder [33]. Since the elastic limit pressure of the shell is obtained based on the stress components, to predict precise pressure, HSDT is used to have accurate elastoplastic results.

The following assumptions are performed for the elastoplastic analysis of the cylindrical structure:

- Strains are small
- The elastic part of the material obeys Hooke's law
- Elastic-perfectly plastic material model is used for simplification of the problem
- The yield stress of the material is changed according to the distance from the inner surface of the cylinder, similar to the other properties of the FGM cylinder
- Plastic flow follows the second invariant of the deviatoric stress tensor (von Mises criterion)

The displacement field for high-order shear deformation theory for axisymmetric cylindrical shell (U_x, U_θ, U_z) is assumed to be a function of z and x; as follows [36]:

$$\begin{cases} U_x(x,z) = \sum u_x^i(x) z^i \\ U_\theta(x,z) = 0 \\ U_z(x,z) = \sum u_z^i(x) z^i \end{cases} \quad (i = 0,1,2,3) \qquad (3)$$

where $u_x^0(x)$ and $u_z^0(x)$ are the displacement components of the mid-plane of the cylinder. Also, $u_x^i(x)$ and $u_z^i(x)$ are the components used to define the displacement change field.

The strain-displacement relations [35] are used to obtain the strain tensor components:

$$\varepsilon_x = \frac{\partial U_x(x,z)}{\partial x}, \varepsilon_\theta = \frac{U_z(x,z)}{r},$$
$$\varepsilon_z = \frac{\partial U_z(x,z)}{\partial z}, \qquad (4)$$
$$\gamma_{xz} = \frac{\partial U_x(x,z)}{\partial z} + \frac{\partial U_z(x,z)}{\partial x}$$

Using the stress-strain relations, the stress tensor for the FG cylindrical shell is written as [35]:

$$\begin{Bmatrix} \sigma_x \\ \sigma_\theta \\ \sigma_z \\ \tau_{xz} \end{Bmatrix} = \frac{E(r)}{(1+\nu)(1-2\nu)} [D] \begin{Bmatrix} \varepsilon_x \\ \varepsilon_\theta \\ \varepsilon_z \\ \gamma_{xz} \end{Bmatrix}$$
$$[D] = \begin{bmatrix} 1-\nu & \nu & \nu & 0 \\ \nu & 1-\nu & \nu & 0 \\ \nu & \nu & 1-\nu & 0 \\ 0 & 0 & 0 & \frac{1-2\nu}{2} \end{bmatrix} \qquad (5)$$

where $E(r)$ denotes Young's Modulus of the shell, which changes through the thickness of the shell. In addition, The stress resultants are written as follows [36]:

$$\begin{Bmatrix} N_x^i \\ N_\theta^i \\ N_z^i \\ N_{xz}^i \end{Bmatrix} = \int_{-h/2}^{h/2} \begin{Bmatrix} \sigma_x(1+z/R) \\ \sigma_\theta R \\ \sigma_z(1+z/R) \\ \tau_{xz}(1+z/R) \end{Bmatrix} z^i \, dz \qquad (6)$$

The strain energy and the external work for a rotating FG cylindrical shell can be written as:

$$U = \frac{1}{2}\sigma_{ij}\varepsilon_{ij}$$
$$W = \iint_S (\vec{f}_{sf}.\vec{u}) dS + \iiint_V (\vec{f}_{bf}.\vec{u}) dV \qquad (7)$$

In Eq. (7), the first and second terms of the external work are associated with the internal pressure and the rotation of the cylinder, respectively.

The variations of strain energy (δU) and the variations of external work (δW) for the shell subjected to the internal pressure are expanded as Eq. (8) [36]:

$$\delta U = 2\pi \int_0^L \int_{-h/2}^{h/2} (\sigma_x \delta\varepsilon_x + \sigma_\theta \delta\varepsilon_\theta + \sigma_z \delta\varepsilon_z + \tau_{xz}\delta\gamma_{xz})(R+z) dz dx$$
$$\delta W = 2\pi \left[\int_0^L (P\delta U_z)\left(R - \frac{h}{2}\right) dx + \int_0^L \int_{-\frac{h}{2}}^{\frac{h}{2}} \rho(r)\omega^2 (R+z)^2 \delta U_Z dz \, dx \right] \qquad (8)$$

$$\frac{d}{dx}(RN_x^i) - iRN_{xz}^{i-1} = 0$$
$$\frac{d}{dx}(RN_{xz}^i) - iRN_z^{i-1} - N_\theta^i = -P\left(R - \frac{h}{2}\right)\left(-\frac{h}{2}\right)^i - \int_{-h/2}^{h/2} \rho(r)\omega^2 (R+z)^2 \, z^i dz, \qquad (i = 0,1,2,3) \qquad (9)$$

Replace the stress and strain components into the variation of strain energy (Eq. (8)), and based on the calculus of variation and virtual work principle ($\delta U = \delta W$), considering the Eq. (6), the governing equations for FGM rotating cylinders are obtained as Eq. (9).

The boundary conditions are as follows:

$$R\left[\sum_{i=0}^{3} N_x^i \delta U_x^i + \sum_{i=0}^{3} N_{xz}^i \delta U_z^i\right]_0^L = 0 \qquad (10)$$

Substituting Eq. (5) into Eq. (6) and doing some calculations, the governing equations are obtained in the form of the displacement as follows:

$$[\bar{A}]\frac{d^2}{dx^2}\{\bar{y}\} + [\bar{B}]\frac{d}{dx}\{\bar{y}\} + [\bar{C}]\{\bar{y}\} = \{\bar{F}\}$$
$$\{\bar{y}\} = \{u_x^0 \;\; u_x^1 \;\; u_x^2 \;\; u_x^3 \;\; u_z^0 \;\; u_z^1 \;\; u_z^2 \;\; u_z^3\}^T \qquad (11)$$

in Eq. (11), $[\bar{A}]_{8\times8}$, $[\bar{B}]_{8\times8}$, and $[\bar{C}]_{8\times8}$ are the coefficients matrices. In addition, $\{\bar{F}\}$ is the force matrix. Eq. (9) is the set of differential equations, and to solve these equations, the reverse of $[\bar{C}]$ is needed, which is irreversible. To overcome this problem, by integrating from the first relation of Eq. (9), it is obtained:

$$RN_x = C_0 \qquad (12)$$

Therefore, Eq. (11) is changed as follows:

$$[A]\frac{d^2}{dx^2}\{y\} + [B]\frac{d}{dx}\{y\} + [C]\{y\} = \{F\}$$
$$\{y\} = \left\{\frac{du_x^0}{dx} \;\; u_x^1 \;\; u_x^2 \;\; u_x^3 \;\; u_z^0 \;\; u_z^1 \;\; u_z^2 \;\; u_z^3\right\}^T \qquad (13)$$

The nonzero components of coefficients matrices [A], [B], and [C] and the components of the force matrix are defined in the Appendix.

The differential Eq. (13) has the solution including the general solution $\{y\}_g$ and particular solution $\{y\}_p$ as:

$$\{y\} = \{y\}_g + \{y\}_p \qquad (14)$$

For the general solution for homogeneous cases, $\{y\}_g = \{V\}e^{mx}$ is substituted in Eq. (13), and it is obtained:

$$e^{mx}[m^2[A] + m[B] + [C]]\{V\} = \{0\} \qquad (15)$$

Eq. (15) is an eigenvalue problem for a non-trivial solution $e^{mx} \neq 0$. The determinant of the coefficient must be considered to be zero.

$$\det[m^2[A] + m[B] + [C]] = 0 \qquad (16)$$

Eq. (16) leads to a sixteen-order polynomial, which contains seven pairs of conjugated roots and a pair of zero roots.

By calculating eigenvectors $\{V\}_i$ corresponds to eigenvalues, the general solution of Eq. (13) is written as:

$$\{y\}_g = \sum_{i=1}^{14} C_i \{V\}_i e^{m_i x} \qquad (17)$$

The constants C_i are obtained by applying boundary conditions.

The particular solution for Eq. (13) is obtained as follows:

$$\{y\}_p = [C]^{-1}\{F\} \qquad (18)$$

Thus the solution of Eq. (13) is achieved by summation of general and particular solutions as:

$$\{y\} = \sum_{i=1}^{14} C_i \{V\}_i e^{m_i x} + [C]^{-1}\{F\} \qquad (19)$$

Finally, u_x^0 is obtained as follows:

$$u_x^0 = \int_0^L \left(\frac{du_x^0}{dx}\right) dx + C_{15} \qquad (20)$$

There are sixteen constants (C_0 to C_{15}) in Eq. (19), and sixteen boundary conditions for the clamped-clamped cylinder are obtained by putting u_x^0, u_x^1, u_x^2, u_x^3, u_z^0, u_z^1, u_z^2, u_z^3 equal to zero at each end of the cylinder ($x = 0$ and $x = L$). After finding the displacement components, the displacement fields and, consequently the strain and stress components are determined. It is assumed that the cylinder is made of elastic-perfectly plastic material. Hence, until the effective stress of any point of the shell is smaller than the yield stress, the shell is elastic. Otherwise, the shell becomes plastic.

The effective stress for the full axisymmetric cylindrical shell based on the von Mises failure theory is defined as [37]:

$$\sigma_e \equiv \frac{1}{\sqrt{2}}[(\sigma_z - \sigma_\theta)^2 + (\sigma_\theta - \sigma_x)^2 + (\sigma_z - \sigma_x)^2 + 6\tau_{zx}^2)]^{1/2} \qquad (21)$$

In addition, the yield function for the material without hardening is defined by [37]:

$$f = \sigma_e - \sigma_y(r) \qquad (22)$$

here σ_y is the yield limit, and it changes gradually through the thickness of the cylinder as Eq. (2). In the above equation, if $f < 0$, the material experiences elastic deformation, while if $f = 0$, the material experiences plastic deformation.

To determine the state of the cylinder (elastic or plastic), it is necessary to find the elastic limit pressure. Exactly after this critical pressure, the state of the cylinder material changes to plastic. For this purpose, it is assumed that the elastic strain is equal to the total strain of the current increment, less the plastic strain of the previously converged increment. The stress tensor computed in this way is called the trial stress tensor. If the trial stress is smaller than the yield stress at the studied point of the cylindrical shell, the cylinder is in an elastic state. Otherwise, it is in the plastic form. After the shell becomes

plastic, the von Mises stress is placed outside the yield surface. Hence, the trial stress increment, $\sigma^{tr}_{t+\Delta t}$, is outside the yield surface. At this stage, the plastic corrector factor is used to update the stress and return it to the yield surface. In the deviatoric plane, the von Mises yield surface became the circle. Based on the normality condition of the yield surface, the plastic corrector factor direction is towards the center of the circle. Hence, this procedure is known as the radial return method. After this, all amounts are represented to be at the end of the time step. Therefore, σ is the updated stress at time $t + \Delta t$, and σ_t denotes the stress at the beginning of the time step.

Hooke's law in the multi-axial form in the state of strain and stress tensors can be expressed as:

$$\tilde{\sigma} = 2G\tilde{\varepsilon}^e + \lambda \,\mathrm{tr}(\tilde{\varepsilon}^e)\tilde{I} \tag{23}$$

where λ and G are the Lamé parameters which are functions of radial position and are described as follows:

$$\begin{aligned} \lambda &= E(r)\nu/(1+\nu)(1-2\nu) \\ G &= E(r)/2(1+\nu) \end{aligned} \tag{24}$$

The total elastic strain is expressed as follows:

$$\tilde{\varepsilon}^e = \tilde{\varepsilon}^e_t + \Delta\tilde{\varepsilon}^e = \tilde{\varepsilon}^e_t + (\Delta\tilde{\varepsilon} - \Delta\tilde{\varepsilon}^p) \tag{25}$$

Substituting Eq. (25) into Eq. (23) and considering the plastic incompressibility of the material condition ($tr(\Delta\tilde{\varepsilon}^p) = 0$), at the end of the time step, the stress tensor may be written as:

$$\begin{aligned} \tilde{\sigma} = 2G(\tilde{\varepsilon}^e_t + \Delta\tilde{\varepsilon}) + \lambda \,\mathrm{tr}(\tilde{\varepsilon}^e_t + \Delta\tilde{\varepsilon})\tilde{I} \\ - 2G\Delta\tilde{\varepsilon}^p \end{aligned} \tag{26}$$

The first two terms of Eq. (26) are denoted as the trial stress tensor ($\tilde{\sigma}^{tr}$), and the last term is considered as the plastic corrector.

Based on the associated flow rule and the assumption that the plastic strain increase is in the same direction as the tangential normal to the yield surface, the plastic strain increment may be written as the von Mises yield criterion as follows [32]:

$$\Delta\tilde{\varepsilon}^p = \frac{3}{2}\Delta p \,\frac{\tilde{\sigma}'}{\sigma_e} \tag{27}$$

Δp denotes effective plastic strain increment and σ˜' represents deviatoric stress tensor.

By replacing Eq. (27) with Eq. (26) expressing the stress in its deviatoric and mean form, and rearranging Eq. (26), it is obtained:

$$\left(1 + 3G\frac{\Delta p}{\sigma_e}\right)\tilde{\sigma}' = \tilde{\sigma}^{tr} - \frac{1}{3}(\tilde{\sigma} : \tilde{I})\tilde{I} \tag{28}$$

With doing some algebra, it can be demonstrated that the right side of Eq. (28) is equal to the deviatoric of the trial stress [31]. Therefore, Eq. (28) is rewritten as:

$$\left(1 + 3G\frac{\Delta p}{\sigma_e}\right)\tilde{\sigma}' = \tilde{\sigma}^{\mathrm{tr}'} \tag{29}$$

By doing the contracted tensor product of each side of Eq. (29) with itself, it is finally obtained [32]:

$$\sigma_e + 3G\,\Delta p = \sigma^{\mathrm{tr}} \tag{30}$$

Substituting Eq. (30) into the yield function for the elastic-perfectly plastic material (Eq. (22)), the effective plastic strain increment and more on the stress tensor can be obtained as:

$$\begin{aligned} \Delta p &= \frac{\sigma^{\mathrm{tr}} - \sigma_y(r)}{3G} \\ \tilde{\sigma} &= \tilde{\sigma}^{tr} - 3G\,\Delta p\,\frac{\tilde{\sigma}'}{\sigma_e} \end{aligned} \tag{31}$$

4. Results and Discussion

In this section, the elastoplastic solution of a cylindrical shell made of FGM and with material properties changes through its radial axis and rotates around its longitudinal axis with the angular velocity of ω is investigated. The cylinder has an inner radius of 40 mm, an outer radius of 60 mm, a thickness of 20 mm, and a length of 800 mm. The Poisson's ratio is considered 0.3 and, its changes are neglected for simplicity and small changes compared to other properties. The Young's Modulus, elastic limit, and density of the inner surface of the cylinder are supposed to be 200 GPa, 250 MPa, and 7800 kg/m3, respectively. The material properties increase or decrease through the thickness of the cylinder based on the inhomogeneity constant changes. To avoid the complexity of the results, the inhomogeneity constants of all properties are supposed to be the same.

To show the effectiveness and accuracy of the present study results, the finite element method is performed using Abaqus. The axisymmetric deformable shell is defined to model the half-length of the cylinder due to its symmetric conditions. To model the FGM properties in Abaqus the USDFLD subroutine is used to access material integration point information and the user-defined field is set based on Eq. (2) for each inhomogeneity constant separately. The plastic strain is set to zero at yield stress because of the perfectly plastic material model used for the analytical approach. The boundary conditions for a clamped edge are defined by setting both the edge deflection and edge slope equal to zero. The internal pressure is applied on the inner surface of the cylinder with the desired magnitude and the rotational body force is used to apply the centrifugal force to the cylinder body. The

second-order eight nodes axisymmetric elements with reduced integration, CAX8R, are used to mesh the cylinder. The twenty elements are used in the radial direction to mesh the cylinder. Convergence of the finite element results in a mesh refinement study accomplished by monitoring the von Mises stress at the inner and the outer layers of the cylinder for different numbers of the elements in the radial direction in Fig. 3. This figure illustrates the von Mises stress for the cylinder subjected to internal pressure equal to 70 MPa and rotate with angular velocity 1000 $rad\ /\ s$ around its axis. As shown in Fig. 3, after the twenty elements the results converged approximately.

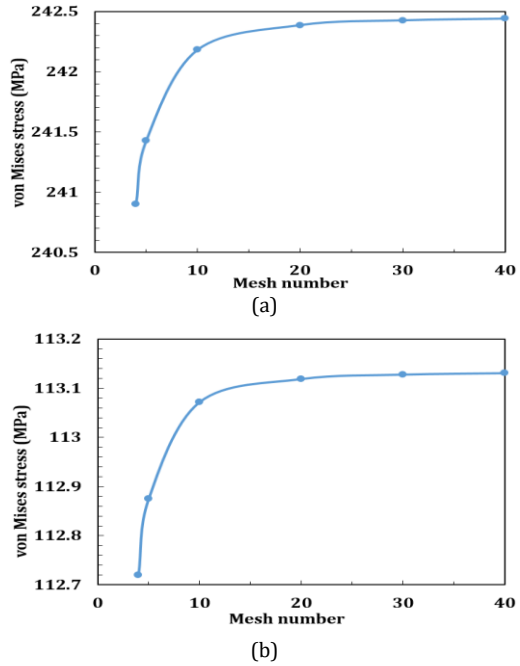

Fig. 3. Convergence of results in mesh refinement study at *x= L/2*, (a) von Mises stress at the inner layer, (b) von Mises stress at the outer layer

Table 1 presents the elastic limit pressure at different lengths of the cylinder for inhomogeneity constants -1, 0, and 1, based on the von Mises yielding criterion. Also, Table 2 shows the elastic limit pressure for changing angular velocity at different cylinder lengths. The error percentage of the present study results with the finite element method (FEM) is calculated using Eq. (32).

$$ERR(\%) = \left(\frac{|P_{FEM} - P_{PS}|}{P_{FEM}}\right) \times 100 \qquad (32)$$

In Eq. (32), P_{FEM} and P_{PS} are the elastic limit pressures obtained using FEM and the present study, respectively.

The yielding occurs at the internal surface of the pressurized cylindrical shell. The results reveal that the elastic limit pressures obtained by the present study have good agreement with the FEM results. The minimum difference between the present study and FEM results occurs away from the boundaries of the cylinder. As shown in Table 1, increasing the inhomogeneity constant leads to an increase in the elastic limit pressure. Although the material properties are the same at the inner surface of the FG cylinder for different inhomogeneity constants, the yielding pressure amount became greater. The reason is that the properties of the other layer of the shell cause the cylinder to become stronger, hence it can tolerate more amount of pressure.

Table 2 shows that increasing angular velocity reduces the amount of the elastic limit pressure. At the mid-length of the cylinder, the elastic limit pressure decreased by almost 2.3, 9.2, and 20.6 percent for angular velocities 500, 1000, and, 1500 $rad\ /\ s$, compared with the no rotation cylinder, respectively.

Table 1. Elastic limit pressure (MPa) for changing inhomogeneity constants at different lengths of the cylinder

	$x = L/2$			$x = L/4$			$x = L/16$			$x = L/40$		
n	FEM	Present study	ERR (%)	FEM	Present study	ERR (%)	FEM	Present study	ERR (%)	FEM	Present study	ERR (%)
-1	68.8	68.58	0.32	68.8	68.59	0.31	73.54	70.86	3.64	105.72	103.91	1.71
0	79.73	80.11	0.48	79.73	80.12	0.49	87.03	83.14	4.47	124.52	121.93	2.08
1	93.48	94.23	0.80	93.48	94.24	0.81	102.95	97.96	4.85	143.32	139.70	2.53

Table 2. Elastic limit pressure (MPa) for changing angular velocity at different lengths of the cylinder

	$x = L/2$			$x = L/4$			$x = L/16$			$x = L/40$		
ω (rad/s)	FEM	Present study	ERR (%)	FEM	Present study	ERR (%)	FEM	Present study	ERR (%)	FEM	Present study	ERR (%)
0	79.73	80.11	0.48	79.73	80.12	0.49	87.03	83.14	4.47	124.52	121.93	2.08
500	77.90	78.28	0.49	77.90	78.30	0.51	84.99	81.15	4.52	122.26	119.62	2.16
1000	72.43	72.81	0.52	72.43	72.82	0.54	79.25	75.62	4.58	117.60	114.91	2.29
1500	63.30	63.67	0.58	63.30	63.69	0.62	69.63	66.37	4.68	109.94	107.07	2.61

Elastic limit pressures through the length of the shell for different inhomogeneity constants are illustrated in Fig. 4. As shown in this figure by increasing the inhomogeneity constant the yielding occurs at higher pressure. The stress concentration at two ends of the cylinder because of clamped-clamped boundary conditions leads to the sudden changes in Fig. 4. These two ends tolerate high stress and thus the elastic limit pressure amounts are significantly smaller than other parts. The elastic limit pressures achieved by the present study, have accurately matched with the FEM ones.

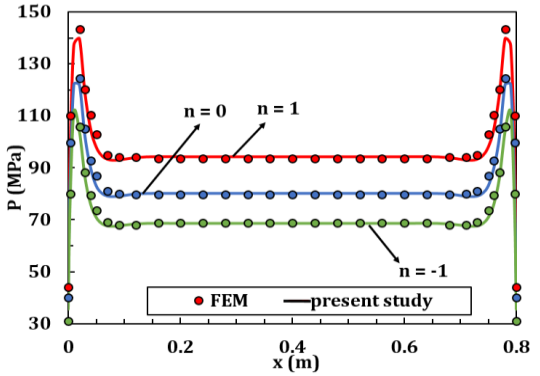

Fig. 4. Elastic limit pressure through the length of the shell for different inhomogeneity constants

Figures 5 and 6 illustrate the circumferential and radial stress distribution through the thickness of the shell at the middle length of it for different inhomogeneity constants, respectively. As shown in these figures the stress distributions of the shell are plotted for the states that the cylinder is yielded at the inner surface $(z = -h/2)$, and $z = -h/4$.

The comparison of the present study stresses concerning FEM stresses reveals that the elastoplastic stress analysis obtained using the present study has acceptable precision. The results show the effectiveness of the HSDT combination with the radial return method in stress analysis of the cylinder in the elastoplastic state.

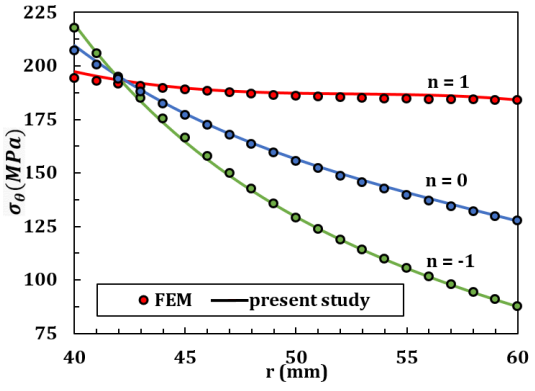

(a)

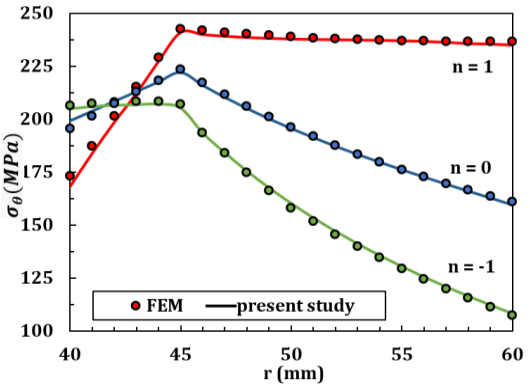

(b)

Fig. 5. Elastoplastic circumferential stress distribution through the thickness of the shell for different inhomogeneity constants, (a) $z = -h/2$, (b) $z = -h/4$

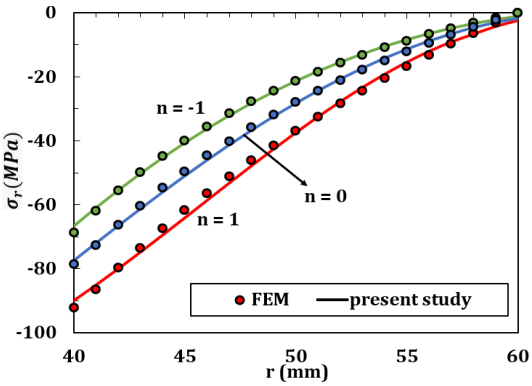

(a)

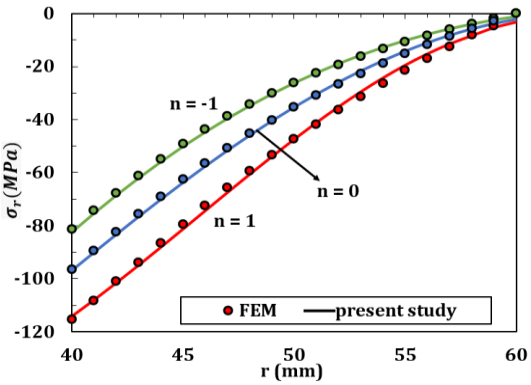

(b)

Fig. 6. Elastoplastic radial stress distribution through the thickness of the shell for different inhomogeneity constants, (a) $z = -h/2$, (b) $z = -h/4$

Figure 7 demonstrates the elastic limit pressures versus angular velocity for inhomogeneity constants -1, 0, and 1 at the mid-length of the shell. As shown in this figure, by increasing the angular velocity of the shell for each inhomogeneity constant, the elastic limit pressure occurs at lower pressure. In addition, increasing the inhomogeneity constant enhances the elastic limit pressure. The dimensionless circumferential and radial stresses (σ_θ/σ_y and σ_r/σ_y) of the FG rotating cylinder at the elastic limit pressure are plotted in Fig. 8. As expected by increasing the angular velocity at a specific

inhomogeneity constant the circumferential and radial stresses are increased and it causes the shell to yield at lower pressure. Also as shown in this figure increasing the inhomogeneity constant leads to a decrease in the circumferential and radial stresses.

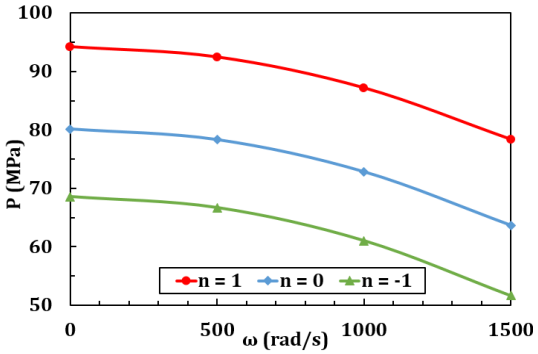

Fig. 7. Effect of angular velocity on elastic limit pressure through the thickness of the shell for different inhomogeneity constants

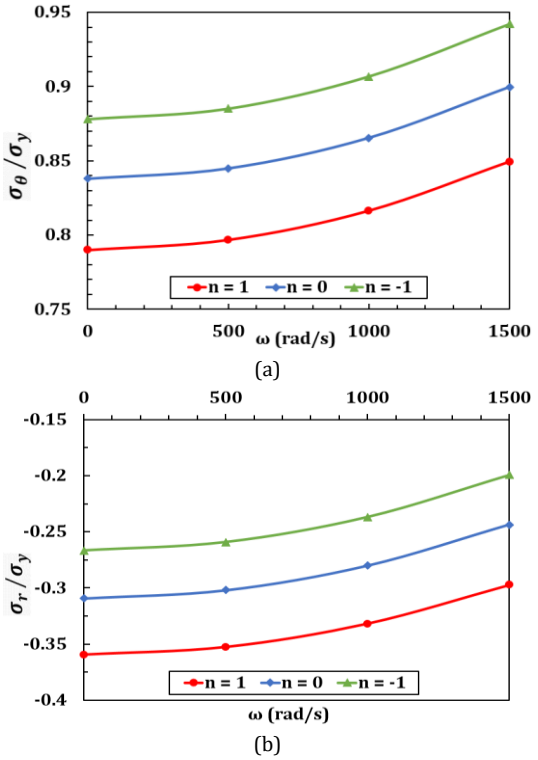

Fig. 8. Dimensionless stress at the elastic limit pressure of the rotating cylinder, (a) circumferential stress, (b) radial stress

5. Conclusions

In this paper, the influence of internal pressure and angular velocity on the elastoplastic behavior of FG thick-walled cylindrical shells is investigated. The cylinder is made of functionally graded material, and the properties of the material, such as Young's Modulus, elastic limit, and density, change gradually from the inner to the outer surfaces. The cylinder is supposed to be axisymmetric and under clamp-clamp boundary conditions. The shell material follows the elastic-perfectly plastic model and the von Mises yield criterion is used to predict the elastic limit pressure. The Prandtl-Reuss flow rule and the radial return mapping method are applied to derive the stress after the cylinder starts the plastic deformation. The following achievements concluded from the present study.

It is shown that the plasticity starts from the inner surface of the rotating cylinder subjected to internal pressure. Thus, it is crucial to predict the trial stress at the inner surface of the shell. As indicated in the present study, high-order shear deformation theory is appropriate to obtain the trial stress tensor to predict the elastoplastic behavior of the cylinder. Despite the Mirsky-Hermann theory (FSDT), the displacement field of HSDT can produce parabolic behavior for shear stress through the thickness direction of the cylinder. Hence, the combination of HSDT with the radial return mapping algorithm has excellent results for elastoplastic stress prediction.

Based on the von Mises yield criterion, the elastic limit pressure occurs at the inner surface through the length of the shell and, it is constant away from the boundaries of the cylinder. Due to stress concentration, the cylinder starts the plastic deformation at the clamped edges.

Although the properties of the inner surface of the cylinder have not changed by increasing the inhomogeneity constant, the elastic limit pressure increased. It is because of increasing the stiffness of the other layers of the cylinder gradually through the length. The stress distribution for the elastoplastic state of the cylinder reveals that the cylinder can tolerate more stress by increasing the inhomogeneity constant.

In addition, elastic limit pressure is highly affected by angular velocity changes. This work is done by centrifugal force, which is proportional to the squared angular velocity of the cylinder.

Controlling the elastoplastic state of the cylinder causes to increase the durability of the final product by inducing residual compressive stresses into the material (Autofrettage). Investigating the elastoplastic behavior of thick-walled cylindrical shells subjected to internal pressure and rotation can help the designer decrease the material usage and reduce the cost of the product.

Conflicts of Interest

The author declares that there is no conflict of interest regarding the publication of this manuscript. In addition, the authors have entirely observed the ethical issues, including plagiarism, informed consent, misconduct, data fabrication and/or falsification, double publication and/or submission, and redundancy.

Appendixes

Nonzero components of coefficients matrices [A], [B], and [C] and the components of the force matrix $\{F\}$ are calculated as follows:

$$A_{22} = (1-\nu)\int_{-h/2}^{h/2} E(r)(R+z)z^2dz$$
$$A_{23} = A_{32} = (1-\nu)\int_{-h/2}^{h/2} E(r)(R+z)z^3dz$$
$$A_{33} = A_{24} = A_{42} = (1-\nu)\int_{-h/2}^{h/2} E(r)(R+z)z^4dz$$
$$A_{34} = A_{43} = (1-\nu)\int_{-h/2}^{h/2} E(r)(R+z)z^5dz$$
$$A_{44} = (1-\nu)\int_{-h/2}^{h/2} E(r)(R+z)z^6dz$$
$$A_{55} = \frac{(1-2\nu)}{2}\int_{-h/2}^{h/2} E(r)(R+z)dz$$
$$A_{66} = \frac{(1-2\nu)}{2}\int_{-h/2}^{h/2} E(r)(R+z)z^2dz$$
$$A_{77} = \frac{(1-2\nu)}{2}\int_{-h/2}^{h/2} E(r)(R+z)z^4dz$$
$$A_{88} = \frac{(1-2\nu)}{2}\int_{-h/2}^{h/2} E(r)(R+z)z^6dz$$
$$A_{56} = A_{56} = \frac{(1-2\nu)}{2}\int_{-h/2}^{h/2} E(r)(R+z)zdz$$
$$A_{57} = A_{75} = \frac{(1-2\nu)}{2}\int_{-h/2}^{h/2} E(r)(R+z)z^2dz$$
$$A_{58} = A_{58} = \frac{(1-2\nu)}{2}\int_{-h/2}^{h/2} E(r)(R+z)z^3dz$$
$$A_{67} = A_{76} = \frac{(1-2\nu)}{2}\int_{-h/2}^{h/2} E(r)(R+z)z^3dz$$
$$A_{68} = A_{86} = \frac{(1-2\nu)}{2}\int_{-h/2}^{h/2} E(r)(R+z)z^4dz$$
$$A_{78} = A_{87} = \frac{(1-2\nu)}{2}\int_{-h/2}^{h/2} E(r)(R+z)z^5dz$$
$$B_{12} = B_{21} = (1-\nu)\int_{-h/2}^{h/2} E(r)(R+z)zdz$$
$$B_{13} = B_{31} = (1-\nu)\int_{-h/2}^{h/2} E(r)(R+z)z^2dz$$
$$B_{14} = B_{41} = (1-\nu)\int_{-h/2}^{h/2} E(r)(R+z)z^3dz$$
$$B_{25} = -B_{52} = (1-\nu)\int_{-h/2}^{h/2} E(r)(R+z)zdz$$
$$B_{25} = -B_{52} = \int_{-h/2}^{h/2} E(r)\left(\nu(R+2z) - \left(\frac{R+z}{2}\right)\right)dz$$
$$B_{26} = -B_{62} = \int_{-h/2}^{h/2} E(r)\left(\nu(2R+3z) - \left(\frac{R+z}{2}\right)\right)zdz$$
$$B_{27} = -B_{72} = \int_{-h/2}^{h/2} E(r)\left(\nu(3R+4z) - \left(\frac{R+z}{2}\right)\right)z^2dz$$
$$B_{28} = -B_{82} = \int_{-h/2}^{h/2} E(r)\left(\nu(4R+5z) - \left(\frac{R+z}{2}\right)\right)z^3dz$$
$$B_{35} = -B_{53} = \int_{-h/2}^{h/2} E(r)\big(\nu(2R+3z) - (R+z)\big)zdz$$
$$B_{36} = -B_{63} = \int_{-h/2}^{h/2} E(r)\big(\nu(3R+4z) - (R+z)\big)z^2dz$$
$$B_{37} = -B_{73} = \int_{-h/2}^{h/2} E(r)\big(\nu(4R+5z) - (R+z)\big)z^3dz$$
$$B_{38} = -B_{83} = \int_{-h/2}^{h/2} E(r)\big(\nu(5R+6z) - (R+z)\big)z^4dz$$
$$B_{45} = -B_{54} = \int_{-h/2}^{h/2} E(r)\left(\nu(3R+4z) - \frac{3}{2}(R+z)\right)z^2dz$$
$$B_{46} = -B_{64} = \int_{-h/2}^{h/2} E(r)\left(\nu(4R+5z) - \frac{3}{2}(R+z)\right)z^3dz$$
$$B_{47} = -B_{74} = \int_{-h/2}^{h/2} E(r)\left(\nu(5R+6z) - \frac{3}{2}(R+z)\right)z^4dz$$
$$B_{48} = -B_{84} = \int_{-h/2}^{h/2} E(r)\left(\nu(6R+8z) - \frac{3}{2}(R+z)\right)z^5dz$$
$$C_{11} = (1-\nu)\int_{-h/2}^{h/2} E(r)(R+z)dz$$
$$C_{22} = -\frac{(1-2\nu)}{2}\int_{-h/2}^{h/2} E(r)(R+z)dz$$
$$C_{33} = -2(1-2\nu)\int_{-h/2}^{h/2} E(r)(R+z)z^2dz$$
$$C_{44} = -\frac{9(1-2\nu)}{2}\int_{-h/2}^{h/2} E(r)(R+z)z^4dz$$
$$C_{23} = C_{32} = -(1-2\nu)\int_{-h/2}^{h/2} E(r)(R+z)zdz$$
$$C_{24} = C_{42} = -3\frac{(1-2\nu)}{2}\int_{-h/2}^{h/2} E(r)(R+z)z^2dz$$
$$C_{34} = C_{43} = -3(1-2\nu)\int_{-h/2}^{h/2} E(r)(R+z)z^3dz$$
$$C_{55} = -(1-\nu)\int_{-h/2}^{h/2} E(r)\left(\frac{1}{R+z}\right)dz$$
$$C_{66} = \int_{-h/2}^{h/2} E(r)(R^2\nu - R^2 - 2Rz - 2z^2)\left(\frac{1}{R+z}\right)dz$$
$$C_{77} = \int_{-h/2}^{h/2} E(r)(4R^2\nu + 4R\nu z + \nu z^2 - 4R^2 - 8Rz - 5z^2)\left(\frac{z^2}{R+z}\right)dz$$
$$C_{88} = \int_{-h/2}^{h/2} E(r)(9R^2\nu + 12R\nu z + 4\nu z^2 - 9R^2 - 18Rz - 10z^2)\left(\frac{z^4}{R+z}\right)dz$$
$$C_{15} = -C_{51} = \nu\int_{-h/2}^{h/2} E(r)dz$$
$$C_{16} = -C_{61} = \nu\int_{-h/2}^{h/2} E(r)(R+2z)dz$$
$$C_{17} = -C_{71} = \nu\int_{-h/2}^{h/2} E(r)(2R+3z)zdz$$
$$C_{18} = -C_{81} = \nu\int_{-h/2}^{h/2} E(r)(3R+4z)z^2dz$$
$$C_{56} = C_{65} = -\int_{-h/2}^{h/2} E(r)\frac{(R\nu+z)}{R+z}dz$$
$$C_{57} = C_{75} = -\int_{-h/2}^{h/2} E(r)\frac{(2R\nu+\nu z+z)}{R+z}dz$$
$$C_{58} = C_{85} = -\int_{-h/2}^{h/2} E(r)\frac{(3R\nu+2\nu z+z)}{R+z}dz$$
$$C_{67} = C_{76} = \int_{-h/2}^{h/2} E(r)(2R^2\nu + R\nu z - 2R^2 - 4Rz - 3z^2)\left(\frac{z}{R+z}\right)dz$$
$$C_{68} = C_{86} = \int_{-h/2}^{h/2} E(r)(3R^2\nu + 2R\nu z - 3R^2 - 6Rz - 4z^2)\left(\frac{z^2}{R+z}\right)dz$$
$$C_{78} = C_{87} = \int_{-h/2}^{h/2} E(r)(6R^2\nu + 7R\nu z + 2\nu z^2 - 6R^2 - 12Rz - 7z^2)\left(\frac{z^3}{R+z}\right)dz$$
$$\{F\} = \frac{1}{\Lambda}\Bigg[C_0 \quad 0 \quad 0 \quad 0 \quad -P\left(R-\frac{h}{2}\right) - \int_{-\frac{h}{2}}^{\frac{h}{2}}\rho\omega^2(R+z)^2dz \quad -P\left(R-\frac{h}{2}\right) - \int_{-\frac{h}{2}}^{\frac{h}{2}}\rho\omega^2(R+z)^2dz$$

$$-P\frac{h^2}{4}\left(R-\frac{h}{2}\right)-\int_{-\frac{h}{2}}^{\frac{h}{2}}\rho\omega^2(R+z)^2z^2dz$$

$$-P\frac{h^2}{4}\left(R-\frac{h}{2}\right)-\int_{-\frac{h}{2}}^{\frac{h}{2}}\rho\omega^2(R+z)^2z^2dz$$

$$P\frac{h^3}{8}\left(R-\frac{h}{2}\right)-\int_{-\frac{h}{2}}^{\frac{h}{2}}\rho\omega^2(R+z)^2z^3dz\Bigg]$$

where,

$$\Lambda=\frac{1}{(1+\nu)(1-2\nu)}\,,\qquad E(r)=E_i\left(\frac{R+z}{r_i}\right)^n$$

References

[1] Saleh, B., Jiang, J., Fathi, R., Al-hababi, T., Xu, Q., Wang, L., Song, D. and Ma, A., 2020. 30 Years of functionally graded materials: An overview of manufacturing methods, Applications and Future Challenges. *Composites Part B: Engineering*, *201*, 108376.

[2] Bai, Y. and Jin, W.L. 2015. Marine Structural Design. 2nd Edition, Butterworth-Heinemann.

[3] Gould, P.L. and Feng, Y. 2018. Introduction to linear elasticity. 4th Edition, Springer, Switzerland.

[4] Calladine, C.R. 2007. Theory of shell structures. Cambridge University Press, New York.

[5] Ghannad, M. and Zamani-Nejad, M., 2012. Complete elastic solution of pressurized thick cylindrical shells made of heterogeneous functionally graded materials. *Mechanika*, *18*(6), pp.640-649.

[6] Mirsky, I. and Herrmann, G., 1958. Axially symmetric motions of thick cylindrical shells. *Journal of Applied Mechanics*, *25*, pp.97-102.

[7] Reddy, J. and Liu, C., 1958. A higher-order shear deformation theory of laminated elastic shells. *International Journal of Engineering Science*, *23*(3), pp.319-330.

[8] Ghannad, M. and Zamani-Nejad, M., 2012. Elastic analysis of heterogeneous thick cylinders subjected to internal or external pressure using shear deformation theory. *Acta Polytechnica Hungarica*, *9*(6), pp.117-136.

[9] Eipakchi, H.R., Rahimi, G.H. and Khadem, S.E., 2003. Closed form solution for displacements of thick cylinders with varying thickness subjected to non-uniform internal pressure. *Structural Engineering and* Mechanics, *16*(6), pp.731-748.

[10] Eipakchi, H.R., Khadem, S.E. and Rahimi, G.H., 2008. Axisymmetric stress analysis of a thick conical shell with varying thickness under nonuniform internal pressure. *Journal of Engineering Mechanics*, *134*(8), pp.601-610.

[11] Ghannad, M. and Gharooni, H., 2012. Displacements and stresses in pressurized thick FGM cylinders with varying properties of power function based on HSDT. Journal of Solid Mechanics, *4*(3), pp.237-251.

[12] Ghannad, M., Zamani-Nejad, M., Rahimi, G.H. and Sabouri, H., 2012. Elastic analysis of pressurized thick truncated conical shells made of functionally graded materials. Structural Engineering and Mechanics, *43*(1), pp.105-126.

[13] Ghannad, M., Rahimi, G.H. and Zamani-Nejad, M. 2013. Elastic analysis of pressurized thick cylindrical shells with variable thickness made of functionally graded materials. Composites Part B: Engineering, *45*(1), pp.388-396.

[14] Jabbari, M., Zamani-Nejad, M. and Ghannad, M. 2015. Thermo-elastic analysis of axially functionally graded rotating thick cylindrical pressure vessels with variable thickness under mechanical loading. *International Journal of Engineering Science*, *96*(1), pp.1-18.

[15] Gharooni, H. and Ghannad, M. 2019. Nonlinear analytical solution of nearly incompressible hyperelastic cylinder with variable thickness under non-uniform pressure by perturbation technique. Journal of Applied and Computational Mechanics, *50*(2), pp.395-412.

[16] Gharooni, H. and Ghannad, M. 2019. Nonlinear analysis of radially functionally graded hyperelastic cylindrical shells with axially-varying thickness and non-uniform pressure loads based on perturbation theory. *Journal of Applied and Computational Mechanics*, *50*(2), pp.324-340.

[17] Parhizkar Yaghoobi, M. and Ghannad M. 2021. Electro-Elastic Analysis of Finite Length FGPM Cylinders Subjected to Electromechanical Loading Using First-Order Electric Potential Theory. *Mechanics of Advanced Composite Structures*, *8* pp.5-31.

[18] Nadai, A. 1950. Theory of fracture and flow of solids. McGraw-Hill, New York.

[19] Chakrabarty, J. 2006. Theory of plasticity. 3rd Edition, Elsevier, UK.

[20] Eraslan, A.N. 2003. On the linearly hardening rotating solid shaft, *European Journal of Mechanics - A/Solids*, *22*(2), pp.295-307.

[21] Eraslan, A.N. 2003. Elastoplastic deformations of rotating parabolic solid disks using Tresca's yield criterion. European Journal of Mechanics-A/Solids, 22(6), pp.861-874.

[22] Prokudin, A. 2020. Exact elastoplastic analysis of a rotating cylinder with a rigid inclusion under mechanical loading and unloading. *ZAMM-Journal of Applied Mathematics and Mechanics*, *100*(3).

[23] Zamani-Nejad, M., Rastgoo, A. and Hadi, A. 2014. Exact elastoplastic analysis of rotating disks made of functionally graded materials. *International Journal of Engineering Science*, *85*, pp.47-57.

[24] Zhu, Q., Wang, S., Zhang, D.F., Jiang, Y.J. and Yue, X. 2020. Elastoplastic analysis of ultimate bearing capacity for multilayered thick-walled cylinders under internal pressure. *Strength of Materials*, *52*(4), pp.521-531.

[25] Temesgen, A., Singh, S. and Pankaj, T. 2021. Elastoplastic analysis in functionally graded thick-walled rotating transversely isotropic cylinder under a radial temperature gradient and uniform pressure. *Mathematics and Mechanics of Solids*, *26*(1), pp.5-17.

[26] Zamani-Nejad, M., Alamzadeh, N. and Hadi, A. 2018. Thermoelastoplastic analysis of FGM rotating thick cylindrical pressure vessels in linear elastic-fully plastic condition. *Composites Part B: Engineering*, 154, pp.410-422.

[27] Ebrahimi T., Zamani-Nejad, M., Jahankohan, H. and Hadi, A. 2021. Thermoelastoplastic response of FGM linearly hardening rotating thick cylindrical pressure vessels. *Steel and Composite Structures*, 38(2), pp.189-211.

[28] Scalet, G. and Auricchio, F. 2018. Computational methods for elastoplasticity: An overview of conventional and less-conventional approaches. *Archives of Computational Methods in Engineering*, *25*(3), pp.545-589.

[29] Wilkins, M.L. 1963 Calculation of elastic-plastic flow. DTIC Document, California.

[30] Loret, B. and Prevost, J.H. 1986. Accurate numerical solutions for Drucker-Prager elastic-plastic models. *Computer Methods in Applied Mechanics and Engineering*, *54*(3), pp.259-277.

[31] Yoder, P. and Whirley, R. 1984. On the numerical implementation of elastoplastic models. *Journal of Applied Mechanics*, *51*(2), pp.283-288.

[32] Dunne, F. and Petrinic, N. 2006. Introduction to computational plasticity. Oxford University Press, New York.

[33] Widłak, G. 2010. Radial return method applied in thick-walled cylinder analysis. *Journal of Theoretical and Applied Mechanics*, *48*(2), pp.381-395.

[34] Kang, Z., Tortorelli, D.A. and James, K.A. 2022. Parallel projection-An improved return mapping algorithm for finite element modeling of shape memory alloys. *Computer Methods in Applied Mechanics and Engineering*, *389*.

[35] Guenaneche, B., Tounsi, A. and Adda Bedia, E. 2014. Effect of shear deformation on interfacial stress analysis in plated beams under arbitrary loading. *International Journal of Adhesion and Adhesives*, *48*, pp.1-13.

[36] Gharooni, H., Ghannad, M. and Zamani-Nejad, M. 2016. Thermo-elastic analysis of clamped-clamped thick FGM cylinders by using third-order shear deformation theory. *Latin American Journal of Solids and Structures*, *13*, pp.750-774.

[37] Mendelson, A. 1968. Plasticity theory and application. Macmillan, New York.